Tectonic signals documented in gravel and silt beds: A comprehensive review of the eastern Tibetan Plateau

Wei Shi [a], Hanchao Jiang [a,b,c*], G. Ian Alsop [d]

[a] *State Key Laboratory of Earthquake Dynamics, Institute of Geology, China Earthquake Administration, Beijing 100029, China*

[b] *Lhasa Geophysical National Observation and Research Station, Institute of Geology, China Earthquake Administration, Beijing 100029, China*

[c] *Xinjiang Pamir Intracontinental Subduction National Field Observation and Research Station, Beijing 100029, China*

[d] *Department of Geology and Geophysics, School of Geosciences, University of Aberdeen, UK*

*** Corresponding author**.

E-mail address: hcjiang@ies.ac.cn (H.C. Jiang).

Abstract

Extracting tectonic signals from sediments in tectonically active areas is important for revealing the history of regional tectonic activity. However, in previous studies, tectonic and climatic signals have often been confused. In this study, we discuss the tectonic signals recorded in Quaternary sediments on the eastern Tibetan Plateau, combined with the geological, geomorphic, regional climate and geographical settings, and summarize six aspects of the sedimentary characteristics of tectonically generated gravels related to seismic landslides, providing an effective reference for other tectonically active areas. In addition, earthquakes commonly cause intermittent changes in the availability of fine particles in provenance areas, which is the rationale for revealing seismic events through a high-resolution sedimentary sequence from which hydrological fluctuations can not be easily identified. The tectonic control of Quaternary sedimentation on the eastern Tibetan Plateau has improved the previous crude understanding of water flow genesis and is of considerable significance for extending research on tectonic activity and assessing seismic hazards.

Keywords: Gravel accumulation; Silt deposition; Tectonic signals; Eastern Tibetan Plateau; Tectonically active areas

1. Introduction

Earth-surface processes in tectonically active regions operate across erosion-dominated landscapes and deliver sediments to depositional systems that can be preserved, consequently documenting environmental changes (Romans et al., 2016). This source-to-sink sediment transfer can be traced to explain the environmental forcing, including tectonism and climate change, in tectonically active regions.

Tectonic signals are present in many areas where exposed and deformed bedrock has experienced severe tectonic activity, such as alpine valleys; however, tectonic information, including timing and intensity, is difficult to obtain. Only a small number of late Quaternary fluvio-lacustrine sequences, which commonly appear less affected by faulting activity, distributed in these areas, making it difficult to study seismic activity through trenching (Jiang et al., 2014, 2017). However, sedimentary stratigraphy represents the best direct manner to unravel tectonic activity on the macro- and micro-scales through the systematic constraints of chronology and tectonic signal inversion from the sediment routing system (Hu et al., 2016; Jiang et al., 2022).

Gravel accumulation preserved within stratigraphic sequences has a long-term generic link with tectonic activity (Burbank and Reynolds, 1984; Schwartz and Coppersmith, 1984; Yeats and Prentice, 1996), including frequent earthquakes along the range-front fault of the Helan Mountains (Deng and Liao, 1996), Jiaocheng fault zone (Xie et al., 2008), northern Zhongtiaoshan fault in Shanxi Province (Si et al., 2014), and northern Tianshan fault in Xinjiang Province (Deng et al., 1996; Deng and Zhang, 2000). Gravels accumulation is generally associated with earthquake shaking (Rinat et al., 2014; Jiang et al., 2016).

Quaternary alluvial gravel and gravelly sediments occur in liquefaction-induced structures in NE Brazil and have been interpreted to be related to seismic shaking (Bezerra et al., 2005; Fortuin and Dabrio, 2008). These gravel clasts and beds are usually oriented (Anand and Jain, 1987) and occasionally interbedded with loess (Deng and Liao, 1996). Chaotic and sporadic gravels have been used to reveal tectonic events (Deng et al., 1996; Jiang et al., 2016; Shi et al., 2022a). Gravel accumulations near active faults are not considered to be genetically related to sedimentary processes (Anand and Jain, 1987).

In addition to gravel clasts and beds, silt deposition in tectonically active regions is often linked to seismic activity in two ways: soft sediment deformation (SSD, Alsop and

Marco, 2011, 2013; Xu et al., 2015; Jiang et al., 2016; Liang et al., 2021; Alsop et al., 2022) and an abrupt increase in silt abundance (Jiang et al., 2014, 2017; Liang and Jiang, 2017; Shi et al., 2022a).

SSD structures related to liquefaction and/or fluidization can be used to reveal paleoseismic events (e.g., Sims, 1975; Obermeier et al., 1991; Marco and Agnon, 1995; Li et al., 1996; Sukhija et al., 1999; Levi et al., 2006). Data on the intensity of earthquakes and their effects on sediments suggest that liquefaction is generally produced when $M_s \geq 5.0/5.5$ (Atkinson, 1984; Galli, 2000). The 2008 M_s 8.0 Wenchuan earthquake triggered > 56000 landslides, covering a total area of > 396 km^2 (Dai et al., 2011; Li et al., 2014) or 197,481 landslides, covering an area of approximately 1160 km^2 (Xu et al., 2012). These landslides caused a large dust storm that deposited dust in nearby lakes (Jiang et al., 2017; Jing et al., 2023) as well as exposed large quantities of silt particles that had accumulated on mountain slopes (Ren et al., 2018b). Based on provenance analysis, fine-grained silt is believed to have been re-transported by ubiquitous strong winds and deposited in ancient Diexi Lake, which records many seismic events (Jiang et al., 2014, 2017; Liang and Jiang, 2017; Shi et al., 2022a).

However, gravel accumulation and silt stratigraphy in tectonically active regions are also related to flood events (Ma et al., 2018; Liu et al., 2019) and lake water-level fluctuations (Xu et al., 2020), respectively. This potentially makes the extraction of tectonic signals from sedimentary formations ambiguous and requires an in-depth and detailed analysis.

In this review, we focus on the eastern Tibetan Plateau (TP) as our target area. Geological and geographical settings were systematically explored and analyzed to develop a sediment routing system that was as objective as possible. Gravel accumulation and silt deposition in the eastern TP are detailed and addressed in the context of aridity and active tectonism. Considering the particular characteristics of earthquakes and landslide hazards is an essential precursor to the development of earthquake-and-dryland-centered policy options that can aid mitigation and preparedness strategies and therefore improve the well-being of populations living in seismically and tectonically active drylands.

2. Geological and geographical settings

The Wenchuan earthquake struck Sichuan Province in southwest China, although the Longmenshan fault zone that hosted the earthquake deformed very slowly and had previously been assigned a modest-to-low seismic hazard rating (Zhang, 2013). This has prompted extensive scientific research into how such earthquakes may be inextricably linked to the distinct geological and geographical backgrounds of a region.

(Insert Figure 1 here)

2.1. Geological settings

The eastern TP has experienced long-term uplift and eastward enlargement. This area has numerous geological features that are atypical of active convergent mountain belts (Burchfiel et al., 2008). The first is the presence of the most notable examples of topographic relief on Earth (> 4 km relief; Fig. 1) but with an absence of large-magnitude low-angle thrust faults (Burchfiel et al., 2008; Kirby et al., 2008; Zhang et al., 2010). Crustal thickening beneath the eastern TP occurred without large-scale shortening of the upper crust but was instead caused by ductile thickening of the deep crust (Burchfiel et al., 2008; Liu et al., 2014; Wang and Shen, 2020). Second, the modern high topography of Longmenshan and the eastern plateau was probably not established until the Late Cenozoic (approximately 15 Ma; Kirby et al., 2002; Clark et al., 2005; Ouimet, 2007). The exposed bedrock in the study area is dominated by Silurian phyllite, quartz schist, Triassic phyllite, and metamorphosed sandstone, which display general deformation and fragmentation features in the field. Third, global positioning system (GPS) observations generally show low shortening rates in the eastern TP (<3 mm/year; Gan et al., 2007; Burchfiel et al., 2008; Zhang et al., 2010; Zhang, 2013) (Fig. 1). Fourth, over geological timescales, individual faults in the Longmenshan fault zone have slipped at slow rates of <1 mm/year (Densmore et al., 2007). The Late Cenozoic shortening across the Longmenshan zone could be limited to 10–20 km, with folding and faulting mainly accommodating the differential surface uplift between the plateau and the Sichuan Basin (Burchfiel et al., 2008; Parsons et al., 2008; Hubbard and Shaw, 2009).

After the Wenchuan earthquake, four strong earthquakes occurred in the eastern TP: the 2010 M_s 7.1 Yushu earthquake, the 2013 M_s 7.0 Lushan earthquake, the 2017 M_s 7.0 Jiuzhaigou earthquake, and the 2021 M_s 7.4 Maduo earthquake. These earthquakes caused severe and widespread damage to the eastern TP and have been related to tectonic activity within the Bayan Kala fault block since 1995 (Xu et al., 2008, 2009; Deng et al., 2014). Furthermore, eight earthquakes with magnitudes ranging from 6.0 to 8.0 have occurred along the Minjiang and Huya faults since 1900 (Fig. 1), indicating a gradually accelerating release of strain energy (Wen et al., 2009; Sun et al., 2018). Considering that large earthquakes can re-rupture regions that have already ruptured during preceding smaller earthquakes and are probably driven by residual strain following many centuries of smaller earthquakes (Feldl and Bilham, 2006), the Huya and Minjiang faults should be the focus of attention in the future.

(Insert Figure 2 here)

2.2. Geographical setting

The landscape of the study area is dominated by the two major mountain ranges of Minshan and Longmenshan, together with the associated alpine valleys (Fig. 2a). The valleys feeding along the Min River are steep and narrow, with incision depths of 800–3000 m (Kirby and Whipple, 2003; Jiang et al., 2014). Strong earthquakes may result in rock-falls and landslides on valley sides (Keller and Rockwell, 1980; Ren et al., 2018b; Keller and Pinter, 2002). Following the 1933 *M*s 7.5 Diexi earthquake, several landslide-dammed lakes formed in the upper reaches of the Min River, which may store large amounts of information related to the Earth's surface processes, including seismic activity (Wang et al., 2011; Jiang et al., 2014, 2016, 2017).

The climate in the study area shifts from subtropical to cold temperate with increasing latitude and from arid in the river valleys to humid in the high mountains owing to the Foehn effect (Shi et al., 2023). The Diexi Lake area, situated in a sub-frigid, semi-humid highland, has a dry and windy climate with cool summers and cold winters. Large temperature differences occur between day and night, as well as between different areas. The mean annual temperature (MAT) at Maoxian City is 11.2 °C. Although Sandagu and Dujiangyan have a maximum rainfall of 1200 mm/yr (Fig. 2b), the mean annual precipitation is only 490.7 mm in Maoxian County, with 70–90 % of that falling in June–September. The mean annual latent evaporation reaches 1375.7 mm, which is 2.8 times the annual precipitation (Fig. 3). The climate in Diexi is similar to that of Maoxian City, except that Diexi has a lower MAT and stronger winds at higher elevations of 2188 m.

(Insert Figure 3 here)

The vegetation in the study area shows distinct vertical zonation and includes forests, subalpine coniferous forests, subalpine meadows, alpine shrubs, and arid valley shrubs (Zhang et al., 2007; Shi et al., 2020; Xu et al., 2020; Wei et al., 2021). Two factors considerably influence the vegetation distribution and ecological conditions in the study area.

One is an arid and windy climate with a large temperature difference between day and night. The other is active tectonics, characterized by frequent earthquakes (Wang et al., 2011). Strong earthquakes often induce numerous landslides and destroy the vegetation cover in the study area (Xu et al., 2012, 2013; Jiang et al., 2022b). Both factors render the landscape, vegetation, and ecological conditions fragile (Xu et al., 2020; Wei et al., 2021).

3. Gravel characteristics reflecting tectonic activity

Gravel accumulation in nature is genetically related to glaciation, tectonism, and water flow. Here, we mainly focused on water flow and tectonism because they have previously been used to explain many sedimentary records in the upper reaches of the Min River (Ma et al., 2018; Chen et al., 2019; Xu et al., 2020; Zhang et al., 2021), and glaciation rarely affected this part of the eastern TP at 2–3 km elevation.

3.1. Gravels related to glaciation and the effect of water flow

Gravels with a glacial origin usually show typical glacial cracks characterized by a set of parallel cracks with or without tiny displacements, while glacial scratching and ‘saddle pebbles’ can also be observed (Zhang et al., 2016). In many gravel-bed rivers, the downstream fining of the grain size is mainly controlled by hydraulic sorting (according to size, shape, and density) and abrasion (crushing, grinding, splitting, chipping, cracking, and sandblasting during transport) (Moussavi-Harami et al., 2004). Dividing the bed sediment into two populations (sand and gravel) permits realistic and useful predictions of the onset of sediment transport and helps explain the development of abrupt gravel-sand transitions (GSTs) commonly observed in natural rivers (Fig. 4) (Wilcock, 1998).

(Insert Figure 4 here)

Selective transport is the dominant downstream fining mechanism; however, the rates of selective transport in sand-bed rivers are lower than those in gravel-bed rivers (Frings, 2008). Accordingly, GSTs are usually rapid and widely observed in present-day rivers (Singer, 2010; Dubille and Lave, 2015). They can extend spatially from 53 to 75 km in length and remain in a stable position for up to 12 years (David, 1999); these are considered important criteria for judging the behavior of water flow. Experiments suggest that selective deposition of the coarsest clasts, owing to unequal mobility, can produce fining rates comparable to the highest rates observed in nature (Paola et al., 1992a, 1992b; Ferguson et al., 1996; Seal et al., 1997; Ferguson, 2003).

Surface coarsening develops in gravel-bed rivers when the local bedload supply from upstream is less than the ability of the flow to transport that load; therefore, it may be possible to relate the degree of river-bed surface coarsening to the sediment supply (Dietrich et al., 1989). Therefore, the sudden appearance of gravel in the stratigraphy is often related to orogen construction (Dubille and Lave, 2015).

3.2. Gravel accumulation related to tectonism

The dispersal of coarse gravel from the source regions into sedimentary basins is commonly viewed as a hallmark of tectonic activity (Sun et al., 2005; Armitage et al., 2011). The criteria for the recognition of syn-tectonic conglomerates include characteristic architectural patterns, progradation of the gravel front, and the rate of down-system fining (Allen and Heller, 2012). Specifically, on the eastern TP, we identified several features closely related to tectonic generation (e.g., Xu et al., 2015; Zhang et al., 2021). (1) The gravel was uniform and similar in composition to the local bedrock. (2) Transport routing of the gravel front with a decrease in size and thickness was evident and could be readily traced in the field (Fig. 5). (3) The gravel was poorly rounded with almost no sorting (Figs. 5d and

6). (4) Gravel layers were directly overlain by clay-silt-dominated lacustrine layers without GST structures or sedimentary bedding, which are closely related to the selective transport of water flow (Fig. 5). (5) Similar to the reduction in the grain size of sediments moving away from the provenance supply in response to tectonic activity (Armitage et al., 2011), the deformation of earlier deposits caused by gravel progradation changed distinctly from strong at proximal sites (intense V-shaped bending and interlayer sliding; Fig. 5c) to weak at distal locations (disappearance of various deformation features) (Zhang et al., 2021). (6) Soft-sediment deformation caused by earthquakes can be easily observed in the field as another important signal of tectonic activity, such as flame structures at Diexi (Zhang et al., 2021), micro-faults at Diaolin (Xu et al., 2015), and other patterns (Alsop and Marco, 2011, 2013; Wang et al., 2011; Jiang et al., 2016; Alsop et al., 2022).

(Insert Figure 5 here)

Sediment routing systems link erosional and depositional landscapes. Landscape evolution over a wide range of timescales has been translated into a narrative of geological history in tectonically active regions (Allen, 2008; Allen and Heller, 2012). Because facies progradation is time-transgressive, the ages of the same gravel layers vary between locations (Burbank et al., 1988; Jordan et al., 1988; Chen et al., 2002; Sun et al., 2004; Heermance et al., 2007; Charreau et al., 2009; Huang et al., 2010). Accordingly, to obtain the tectonic timing of the causative gravel accumulation event, dynamic framework of the sediment routing system that transports the sediment from the source to the sink within a limited distance must be considered.

Field observations have shown that gravel origins can be spatially traced on the eastern TP (Zhong et al., 2017). Occasionally, no erosion signals were observed between the gravel layer and underlying sediment layers (Xu et al., 2015; Zhang et al., 2021). Considering that a given gravel layer was deposited instantaneously, relative to the slow deposition of fine lacustrine sediments (Figs. 5d and 6; Jiang et al., 2022), the thickness of the gravel layers could be deduced to establish a reliable chronology for the lacustrine sequence (Zhang et al., 2021). Accordingly, recent studies on the eastern TP have provided a suitable and systematic approach for dating tectonic activity characterized by frequent earthquakes (Xu et al., 2015; Zhang et al., 2021).

(Insert Figure 6 here)

3.3. Main contribution of seismic landslides to gravel accumulation

A two-fold increase in erosion coefficients occurs in basins within 15 km of major faults compared to those beyond 15 km, suggesting that tectonic deformation through seismic shaking and rock damage markedly affects the eastern TP erosion and topography (Kirkpatrick et al., 2021). Historical records show that several strong earthquakes occurred in the Diexi area, causing extensive landslide residues in the area (Ren et al., 2018; Zhang et al., 2021). Earthquake-induced landslides are closely related to the magnitude of the earthquake and epicentre distance (Keefer, 1984). Based on the intensity attenuation model and the historical seismic records, a magnitude of $M_s > 7.3$ has been inferred for the gravel accumulation event at Diexi (Zhang et al., 2021), which deserves to be examined across a wider region in the future.

The Xinmocun landslide (Fig. 7) occurred on 24 June, 2017 in Diexi Town, Maoxian County, Sichuan Province, resulting in 83 deaths (Wen et al., 2017). The sliding mass damaged the Songping Gully, with an accumulated body of 13 million m3 (Fan et al., 2017). Xinmocun Village is located near the intersection of the active Minjiang and Songpinggou faults. These faults govern the rock mass characteristics of the Xinmocun landslide slope (Chen and Wu, 2018). Intensive regional tectonic processes dominate the formation of discontinuities in rock masses.

(Insert Figure 7 here)

Field observations revealed three sets of joints (Chen and Wu, 2018). The orientation of the first set was N70°W/51°SW, corresponding to the bedding of the rock formations. The second was a subvertical joint set oriented at N7°E/71°NW. The third set of discontinuities had a gentler dip angle with an orientation of N40°E/29°NW (Su et al., 2017). The Xinmocun landslide occurred in the same area as the 1933 Diexi earthquake (Xu et al., 2017). The main causes of fracture extension and slope destabilization are physical and chemical erosion caused by rainfall, the accumulation of seismic effects, and frozen groundwater in winter (Su et al., 2017; Wen et al., 2017). A low-intensity and long-duration period of rainfall occurred 24 days before the landslide (Su et al., 2017). The cumulative rainfall in June of the year of the Xinmocun landslide was 78–100 mm, which was 42% above the average rainfall in June (Wen et al., 2017). The Diexi earthquake and subsequent intense earthquakes disturbed and extended the fractures in the longitudinal and vertical directions, damaging the sliding rock mass (Su et al., 2017). This provided the preconditions and fundamental reasons for the Xinmocun landslide. Accordingly, a tectonically active geological background is fundamental factor in the investigation and prevention of seismic disasters, including landslides. Similarly, the geological background of the tectonic activity is the most important factor in the analysis of gravel accumulation signals in tectonically active areas.

4. Source characteristics of silt deposition reflecting tectonic activity

4.1. Control of active tectonic activity on silt sources

Eight earthquakes with magnitudes of 6.0–8.0 have occurred around the Minshan uplift zone on the eastern TP since 1900 (Fig. 1; Sun et al., 2018). These frequent earthquakes triggered tens of thousands of landslides (Dai et al., 2011; Xu et al., 2012, 2013) and exposed and remobilized large quantities of fine sediment accumulated on mountain slopes (Jiang et al., 2014). These fine particles were transported by ubiquitous strong winds into nearby lakes, which is evidently reflected in the high-resolution grain size, magnetic susceptibility, and geochemical records of Diexi Lake (Jiang et al., 2014, 2017; Liang and Jiang, 2017). Diexi Lake lies immediately adjacent to the Min River. Suppose the water recharge of the Min River directly affected the water level of Diexi Lake. In that case, this should have been recorded in a coarse-grained to fine-grained sequence, similar to the changes in hydrodynamic capacity reflected by GSTs, specific sedimentary stratigraphic features (oblique bedding, pinnate and bedding), and XRF elemental ratios reflecting climate change. However, these indicators do not reflect climate change or changes in material sources caused by seismic activities (Jiang et al., 2014, 2017; Liang and Jiang, 2017).

The entire lithosphere (crustal and upper mantle rocks) of the eastern TP is relatively weak (Clark et al., 2005; England and Molnar, 1997; Flesch et al., 2001). Constrained by the pushing and extrusion of the Indian Plate and the surrounding rigid mass, the relatively weak lithosphere below the eastern TP shortens and absorbs the squeezing of the Indian Plate, whereas vertical thickening leads to a substantial uplift of the plateau (Zhang et al., 2018). During the uplift process, frequent earthquakes resulted in the fragmentation of weak bedrock (sandstone and limestone) in the upper reaches of the Min River, resulting in multiple sets of cleavages that created the necessary preconditions for subsequent landslides (Chen and Wu, 2018; Su et al., 2017).

The 2008 Wenchuan earthquake triggered several landslides (e.g., Dai et al., 2011; Xu et al., 2012, 2013; Li et al., 2014). These landslides caused a large dust storm that deposited dust in nearby lakes (Jiang et al., 2017; Lv et al., 2023) as well as exposed large quantities of fine-grained sediment that had accumulated on mountain slopes (Jiang et al., 2014; Dai et al., 2021). These clastic particles provided a major sediment source for deposition in nearby lakes, whose records corresponded well with 26 and 70 seismic events in the Diexi and Lixian lacustrine sediments, respectively (Jiang et al., 2014, 2017; Shi et al., 2022a). The seismic event layers in these lacustrine sediments show abrupt coarsening and upward fining of grain size (Jiang et al., 2014, 2017; Shi et al., 2023). In addition, the sand fraction (>63 μm) suddenly increased by 10.4% in response to the 1933 M_s 7.5 Diexi earthquake in the Huojizhai core (Wei et al., 2021). Other lakes worldwide, such as Lake Washington, U.S.A. (Karlin and Abella, 1992); Marmara Sea, Turkey (McHugh et al., 2006); Lake Ellery, New Zealand (Howarth et al., 2016); and Lake Rara, Nepal (Ghazoui et al., 2019), also exhibit consistent grain size characteristics. Analyses of rare earth elements, quartz grains morphology, grain size (Jiang et al., 2014), and major/trace elements (Liang and Jiang, 2017) demonstrated that these lacustrine sediments in the eastern TP were transported by wind into the lakes. Such windblown features of lacustrine sediments are closely related to the overall arid climate and the geomorphological background of strong winds in alpine valleys under the geological background of frequent tectonism in the study area.

4.2. Impact of arid climate on silt deposition

As mentioned earlier, in terms of rainfall, most studies have only considered the source of local rainfall, average annual rainfall, and whether rainfall is mainly concentrated in the summer because these features determine whether rainfall is related to summer monsoons (Jiang and Ding, 2008; Jiang et al., 2011, 2013). However, the eastern TP has specific characteristics, such as the Foehn effect (Fig. 8) (Shi et al., 2023), and approximately 70% of the rainfall occur at night (Fig. 3) (CCLHMQAC, 1997). These characteristics determine the changes in regional rainfalls, floods, and runoff in major rivers.

(Insert Figure 8 here)

The Indian and East Asian summer monsoons mainly influence the eastern TP (Bookhagen and Burbank, 2010; Zhou et al., 2010; Yao et al., 2013; Li et al., 2020; Shi et al., 2020; Zhao et al., 2020). Owing to the alpine valley terrain, the summer monsoon carrying water vapor encounters mountain obstructions, causing condensation and rainfall. By the time it reaches the upper reaches of the Min River, any water vapor is considerably reduced (Fig. 8) (CCLHMQAC, 1997). In addition, the upper reaches of the Min River are located on the leeward slope of the Longmenshan uplift zone, and the Foehn effect is always significant. Airflow crosses the mountain peaks from east to west warms and reduces humidity; therefore, only small amounts of water vapor reach the study area (Fig. 8). Maoxian County was selected as our study locality; it has an annual precipitation of only 490.7 mm (CCLHMQAC, 1997; Jiang et al., 2014, 2015), which is close to the lower limit of rainfall in the sub-humid climate zone (400–800 mm). The local rainy season is from May to September, during which daytime precipitation is 144.8 mm (29.5%) and nocturnal precipitation is 345.7 mm (70.5%). The nocturnal precipitation during the rainy season ranges from 46.0 to 59.2 mm with an average of 52.6 mm (Fig. 3a). Considering that the number of rainfall days varies from 15.3 to 18.7, with an average of 17.3 (Fig. 3b), the mean daily precipitation is only approximately 3.0 mm. Notably, the number of days with daily precipitation $\geq$ 15 mm ranges from 0.5 to 1.5, with an average of 0.86, while daily precipitation $\geq$ 25 mm occurs on an average of 0.28 days (Fig. 3b). This is consistent with the characteristics of how little rainfall has been observed during our annual summer field expeditions since 2008. This also corresponds to no full day of $\geq$ 25 mm of daily rainfall.

The Xiaowa River joins the Min River at Zhenjiangguan, the Heishui River joins the Min River at Lianghekou, and the Zagunao River joins the Min River at Wenchuan (Fig. 2). Statistical analysis of data from 1956 to 1978 revealed that the average annual runoff along the Min River downstream from these three sites varied from 18.4–43.4 × 10^8 m^3, much lower than that of the Zipingpu Reservoir at the entrance to the Sichuan Basin (143.4 × 10^8 m^3). At these sites, no significant increase in the average annual runoff was detected after the tributaries merged (Fig. 2b).

Wenchuan is located at the junction of the northwest Sichuan Plateau and the west Sichuan Basin. The Xuankou-Yingxiu rainstorm area occurs here, and the annual rainfall is ~1300 mm. After the Wenchuan earthquake, four rainstorms occurred on 13 August 2010, 10 July 2013, 20 August 2019, and 10 August 2020. However, 12 years of observations in the epicenter area of the Wenchuan earthquake showed that debris flow and river transport consumed only a small portion of the co-seismic debris, with over 70% of this debris remaining stable on the mountain slopes (Dai et al., 2021). The influence of rainfall on this co-seismic debris was extremely small that the lacustrine facies in Zipingpu Reservoir only began to record the 2008 Wenchuan earthquake event in 2010 (Zhang et al., 2019).

The annual evaporation in the study area reaches 1375.1 mm and is mainly concentrated also in March–September, where it varies between 110.7 and 171.5 mm, with an average of 146.2 mm (Fig. 3a); this is approximately three times greater than the mean monthly precipitation. These characteristics lay the foundation for the overall arid climatic features of the eastern TP, which explain the overall low rainfall and runoff of the upper Min River (Fig. 2b). In this scenario, it is incorrect to attribute the coarsening of silt particles within the lacustrine sediments at Diexi to fluctuations in the water level, as proposed by Xu et al. (2020), because they show a uniform pattern that suddenly becomes coarser, revealing to seismic events (Jiang et al., 2014, 2017; Shi et al., 2022a).

This evidence provides a good explanation for the low probability of flood events in the upper Min River, although the exact probability of flooding could not be determined. Meanwhile, from the upper reaches of the Min River downwards, particularly downstream of Diexi, the slope of the Min Mountains became steeper, the river channel became narrower, and the corresponding tectonic activity was enhanced (Kirby and Whipple, 2003; Shi et al., 2022b). These features are responsible for gravel accumulation (Xu et al., 2015; Zhang et al., 2021) and silt (Jiang et al., 2014, 2017; Shi et al., 2022b) layer deposition related to tectonic activity.

4.3. Impact of geomorphology on silt deposition

The terrain exerts a first-order effect on the surface wind regime (Bromwich and Kurtz, 1984; Parish and Bromwich, 1987; Parish, 1988; Turner et al., 2009). The close coupling between wind and topography allows for the estimation of the former if the latter is known and has evident characteristics (Parish and Bromwich, 1987). Under the blocking effect of large mountains, such as the Min Mountains on the eastern TP, airflow is forced to move along the mountains, creating a guiding effect of mountains on airflow. When the airflow encounters a narrow corridor (or mountain pass) formed by the terrain, the topography guides the airflow as well as produces a “narrow channel effect”, which considerably enhances the wind speed.

(Insert Figure 9 here)

Meanwhile, as sunlight increases during the day, air convection in the valley becomes stronger and reaches its maximum in the afternoon, and the wind speed of the Foehn effect reaches its maximum. This is an evident weather phenomenon that was observed during our annual fieldwork. Statistical analysis of meteorological data from 1953 to 1985 showed that the maximum monthly wind speed in the Maoxian area varied from 12 to 21 m/s, with an average of 15.8 m/s (Fig. 3c). Furthermore, according to the dynamic theory of the atmospheric boundary layer, near-surface wind speeds increase at a logarithmic rate with increasing height (Zhao, 2006), and wind speeds can reach 20.8–24.4 m/s on the eastern TP (Liu, 2014). This increases their ability to carry dust particles from mountain slopes to nearby lakes. The elevation gradually increases upstream along the upper reaches of the Min River, especially from Diexi (Fig. 9). This may explain why the distribution of loess gradually became more extensive along the upper reaches of the Min River, especially from upstream Diexi (Fig. 9).

(Insert Figure 10 here)

Systematic patterns of channel gradients in eastern Tibet show no systematic relationship between the steepness indices and the upstream drainage area (Kirby and Whipple, 2003). The Heishui/Min River system showed a systematic relative increase in gradient in $\times 10^8$ m^2, whereas the Jin River (east of Min Shan) continued to decrease in gradient in the same drainage area (Fig. 10), suggesting that regional differences in concavity are not related to downstream changes in sediment flux (Sklar and Dietrich, 1998). Gradients in the headwater reaches of the Jin River were similar to those along the small tributaries of the lower Min River (Fig. 10), suggesting external control of the channel gradient (Kirby and Whipple, 2003). Channels of all sizes were steeper near the plateau margin, and the steep channel profiles along the topographic front of the plateau reflected an active differential rock uplift between this region and the foreland (Kirby and Whipple, 2003). In addition, the tributaries on the opposite sides of the Min River are asymmetric (Fig. 2). The lower perimeter and area of the drainage sub-basins, total channel length and bifurcation ratio within the eastern flank along the Minjiang mainstream were the result of the Quaternary differential uplift of the Minshan Mountain region (Zhang et al., 2006).

5. Conclusions and future work

We provided a review of the characteristics of gravel accumulation and silt deposition sources on the eastern TP that can indicate regional tectonic signals, combined with a comprehensive analysis of the geological, geomorphic, regional climate, and geographical settings. The literature review, combined with our previous research, highlights the main contribution of the active tectonic activity to debris sources. By analyzing the dynamic characteristics of the source-sink system of the gravel accumulation and silt deposition, we contend that gravel accumulation and silt deposition with uniform sedimentary characteristics are indicative of regional seismic events and summarize six sedimentary characteristics of gravel accumulations related to tectonic genesis. The identification of tectonic gravel accumulation and silt deposition on the eastern TP has corrected the crude understanding that all regional gravel accumulation and silt depositions on the eastern TP have water flow genesis.

The sedimentological characteristics of single-origin gravel are now fairly well understood based on extensive field investigations and experimental studied. However, several questions remain unanswered. Previous studies have focused on the existing features of gravel (such as rounding and sorting) to determine its genesis, neglecting later transformations. For example, angular gravel of glacial and tectonic origin is transformed into rounded gravel through long-term water flow and remains in place throughout this process. Therefore, the attribution of all the rounded gravel in active tectonic areas to water flow causes the omission of tectonic signals from gravel accumulation. In the source-to-sink process, the characteristics of gravel accumulation and clay deposition in the tectonically stable middle and lower reaches of the river are mainly caused by water flow; however, the tectonically active upstream reaches of the river exhibit a mixture of multiple genes. Extracting and summarizing the tectonic signals in these multi-genesis gravel accumulations is important for studying regional tectonic activity. The transformation of the original features and multi-genesis properties of gravel accumulation are the main obstacles to establishing quantitative indicators for tectonic signals. Currently, research on silt deposition in lake deposits is mainly based on multi-index changes to identify paleoseismic events and then establish regional paleoseismic sequences. The use of these event layers (excluding the SSD) to evaluate the seismic intensity and delineate seismic faults will be of considerable significance for future seismic activity assessments.

Data availability

Datasets related to this article are included in the article/ Supplementary files, further inquiries can be directed to the corresponding author.

Acknowledgements

This project was supported by the National Natural Science Foundation of China (42207239) and National Nonprofit Fundamental Research Grant of China, Institute of Geology, China Earthquake Administration (IGCEA1906). We gratefully acknowledge the editors of the journal and the anonymous reviewers for their useful and detailed comments and suggestions to improve the original submission.

Reference

Allen, P.A., 2008. From landscapes into geological history. Nature 451, 274-276. https://doi.org/10.1038/nature06586.

Allen, P.A., Heller, P.L., 2012. Dispersal and preservation of tectonically generated alluvial gravels in sedimentary basins. In: Tectonics of Sedimentary Basins; Recent Advances (C. Busby, A. Azor), pp.111–130. Wiley-Blackwell, Oxford, 647pp. https://doi.org/10.1002/9781444347166.ch6.

Alsop, G.I., Marco, S., 2011. Soft-sediment deformation within seismogenic slumps of the Dead Sea basin. J. Struct. Geol. 33, 433-457. https://doi.org/10.1016/j.jsg.2011.02.003.

Alsop, G.I., Marco, S., 2013. Seismogenic slump folds formed by gravity-driven tectonics down a negligible subaqueous slope. Tectonophysics 605, 48-69. https://doi.org/10.1016/j.tecto.2013.04.004.

Alsop, G.I., Marco, S., Levi, T., 2022. Recognising surface versus sub-surface deformation of soft-sediments: Consequences and considerations for palaeoseismic studies. J. Struct. Geol. 154, 104493. https://doi.org/10.1016/j.jsg.2021.104493.

Anand, A., Jain, A.K., 1987. Earthquakes and deformational structures (seismites) in Holocene sediments from the Himalayan-Andaman Arc, India. Tectonophysics 133, 105-120. https://doi.org/10.1016/0040-1951(87)90284-8.

Armitage, J.J., Duller, R.A., Whittaker, A.C., Allen, P.A., 2011. Transformation of tectonic and climatic signals from source to sedimentary archive. Nat. Geosci. 4, 231-235. https://doi.org/10.1038/ngeo1087.

Atkinson, G., 1984. Simple computation of liquefaction probability for seismic hazard applications. Earthq. Spect. 1, 107-123. https://doi.org/10.1193/1.1585259.

Bezerra, F.H.R., da Fonseca, V.P., Vita-Finzi, C., Lima-Filho, F.P., Saadi, A., 2005. Liquefaction-induced structures in Quaternary alluvial gravels and gravelly sediments, NE Brazil. Eng. Geo. 76, 191-208. https://doi.org/10.1016/j.enggeo.2004.07.007.

Bookhagen, B., Burbank, D.W., 2010. Toward a complete Himalayan hydrological budget: Spatiotemporal distribution of snowmelt and rainfall and their impact on river discharge. J. Geophys. Res. 115, F03019. https://doi.org/10.1029/2009JF001426.

Bromwich, D.H., Kurtz, D.D., 1984. Katabatic wind forcing of the Terra Novabay Polynya. J. Geophys. Res. 89, 3561-3572. https://doi.org/10.1029/JC089iC03p03561.

Burbank, D.W., Beck, R.A., Raynolds, R.G.H., Hobbs, R., Tahirkheli, R.A.K., 1988. Thrusting and gravel progradation in foreland basins: A test of post-thrusting gravel dispersal. Geology 16, 1143-1146. https://doi.org/10.1130/0091-7613(1988)016<1143:TAGPIF>2.3.CO;2.

Burbank, D.W., Reynolds, R.G.H., 1984. Sequential late Cenozoic structural disruption of the northern Himalayan foredeep. Nature 311, 114-118. https://doi.org/10.1038/311114a0.

Burchfiel, B.C., Royden, L.H., van der Hilst, R.D., Hager, B.H., Chen, Z., King, R.W., Li, C., Lu, J., Yao, H., Kirby, E., 2008. A geological and geophysical context for the Wenchuan earthquake of 12 May 2008, Sichuan, People's Republic of China. GSA Today 18, 4-11. https://doi.org/10.1130/GSATG18A.1.

Charreau, J., Gumiaux, C., Avouac, J.P., Augier, R., Chen, Y., Barrier, L., Gilder, S., Dominguez, S., Charles, N., Wang, Q.C., 2009. The Neogene Xiyu Formation, a diachronous prograding gravel wedge at front of the Tianshan: Climatic and tectonic implications. Earth Planet. Sci. Lett. 287, 298-310. https://doi.org/10.1016/j.epsl.2009.07.035.

Chen, J., Burbank, D.W., Scharer, K.M., Sobel, E., Yin, J.H., Rubin, C., Zhao, R.B., 2002. Magnetochronology of the Upper Cenozoic strata in the Southwestern Chinese Tian Shan: rates of Pleistocene folding and thrusting. Earth Planet. Sci. Lett. 195, 113-130. https://doi.org/10.1016/S0012-821X(01)00579-9.

Chen, K.T., Wu, J.H., 2018. Simulating the failure process of the Xinmo landslide using discontinuous deformation analysis. Eng. Geol., 239, 269-281. https://doi.org/10.1016/j.enggeo.2018.04.002.

Chen, R.C., Chen, J., Ma, J.X., Cui, Z.J., 2019. Quartz grain surface microtextures of dam-break flood deposits from a landslide-dammed lake: a case study. Sed. Geol. 383, 238-247. https://doi.org/10.1016/j.sedgeo.2019.02.010.

Clark, M.K., Bush, J.W.M., Royden, L.H., 2005. Dynamic topography produced by lower crustal flow against rheological strength heterogeneities bordering the Tibetan Plateau. Geophys. J. Int. 162, 575-590. https://doi.org/10.1111/j.1365-246X.2005.02580.x.

Clark, M.K., House, M.A., Royden, L.H., Burchfiel, B.C., Whipple, K.X., Zhang, X., Tang, W., 2005. Late Cenozoic uplift of southeastern Tibet. Geology 33, 525-528. https://doi.org/10.1130/G21265.1.

Committee for compiling local history of Maowen Qiang Autonomous County (CCLHMQAC), 1997. Maowen Qiang Autonomous County Chronicle. Aba Tibetan and Qiang Autonomous Prefecture of Sichuan Province, Sichuan Cishu Press, p.1-822.

Dai, F.C., Xu, C., Yao, X., Xu, L., Tu, X.B., Gong, Q.M., 2011. Spatial distribution of landslides triggered by the 2008 Ms 8.0 Wenchuan earthquake, China. J. Asian Earth Sci. 40, 883-895. https://doi.org/10.1016/j.jseaes.2010.04.010.

Dai, L.X., Scaringi, G., Fan, X.M., Yunus, A.P., Liu-Zeng, J., Xu, Q., Huang, R.Q., 2021. Coseismic debris remains in the orogeny despite a decade of enhanced landsliding. Geophys. Res. Lett. 48, e2021GL095850. https://doi.org/10.1029/2021GL095850.

David K.A., 1999. The gravel-sand transition in a disturbed catchment. Geomorphology 27, 325-341. https://doi.org/10.1016/S0169-555X(98)00078-6.

Deng, Q.D., Cheng, S.P., Ma, J., Du, P., 2014. Seismic Activities and Earthquake Potential in the Tibetan Plateau. Chin. J. Geophys. 57, 2025-2042. https://doi.org/10.6038/cjg20140701 (in Chinese with English abstract).

Deng, Q.D., Liao, Y.H., 1996. Paleoseismology along the range-front fault of Helan Mountains, north central China. J. Geophys. Res. 101, 5873-5893. https://doi.org/10.1029/95jb01814.

Deng, Q.D., Zhang, P.Z., 2000. Colluvial wedges associated with pre-historical reverse faulting paleoearthquakes. Sci. Bull. 45, 1598-1604. https://doi.org/10.3321/j.issn:0023-074X.2000.06.020 (in Chinese with English abstract).

Deng, Q.D., Zhang, P.Z., Xu, X.W., Yang, X.P., Peng, S.Z., Feng, X.Y., 1996. Paleoseismology of the northern piedmont of Tianshan Mountains, northwestern China. J. Geophys. Res. 101, 5895-5920. https://doi.org/10.1029/95jb02739.

Densmore, A.L., Ellis, M.A., Li, Y., Zhou, R., Hancock, G.S., Richardson, N., 2007. Active tectonics of the Beichuan and Pengguan faults at the eastern margin of the Tibetan Plateau. Tectonics 26, TC4005. https://doi.org/10.1029/2006TC001987.

Dietrich, W.E., Kirchner, J.W., Ikeda, H., Iseya, F., 1989. Sediment supply and the development of the coarse surface layer in gravel-bedded rivers. Nature 340, 215-217. https://doi.org/10.1038/340215a0.

Dubille, M., Lave, J., 2015. Rapid grain size coarsening at sandstone/conglomerate transition: similar expression in Himalayan modern rivers and Pliocene molasses deposits. Basin Res. 27, 26-42. https://doi.org/10.1111/bre.12071.

England, P., Molnar, P., 1997. Active deformation of Asia: From kinematics to dynamics. Science 278, 647-650. https://doi.org/10.1126/science.278.5338.647.

Fan, X.M., Xu, Q., Scaringi, G., Dai, L.X., Li, WL., Dong, X.J., Zhu, X., Pei, X.J., Dai, K.R., Havenith, H.B., 2017. Failure mechanism and kinematics of the deadly June 24th 2017 Xinmo landslide, Maoxian, Sichuan, China. Landslides, 14, 2129–2146. https://doi.org/10.1007/s10346-017-0907-7

Feldl, N., Bilham, R., 2006. Great Himalayan earthquakes and the Tibetan Plateau. Nature 444, 165-170. https://doi.org/10.1038/nature05199.

Ferguson, R., Hoey, T., Wathen, S., Werritty, A., 1996. Field evidence for rapid downstream fining of river gravels through selective transport. Geology 24, 179-182. https://doi.org/10.1130/0091-7613(1996)024<0179:FEFRDF>2.3.CO;2.

Ferguson, R.I., 2003. Emergence of abrupt gravel to sand transitions along rivers through sorting processes. Geology 31, 159-162. https://doi.org/10.1130/0091-7613(2003)031<0159:EOAGTS>2.0.CO;2.

Flesch, L.M., John Haines, A., Holt, W.E., 2001. Dynamics of the India-Eurasia collision zone. J. Geophys. Res. 106, 16435-16460. https://doi.org/10.1029/2001jb000208.

Fortuin, A.R., Dabrio, C.J., 2008. Evidence for late Messinian seismites, Nijar Basin, south-east Spain. Sedimentology 55, 1595-1622. https://doi.org/10.1111/j.1365-3091.2008.00959.x.

Frings, R.M., 2008. Downstream fining in large sand-bed rivers. Earth Sci. Rev. 87, 39-60. https://doi.org/10.1016/j.earscirev.2007.10.001.

Galli, P., 2000. New empirical relationships between magnitude and distance for liquefaction. Tectonophysics 324, 169-187. https://doi.org/10.1016/S0040-1951(00)00118-9.

Gan, W.J., Zhang, P.Z., Shen, Z.K., Niu, Z.J., Wang, M., Wan, Y.G., Zhou, D.M., Cheng, J., 2007. Present-day crustal motion within the Tibetan Plateau inferred from GPS measurements. J. Geophys. Res. 112, B08416. https://doi.org/10.1029/2005JB004120.

Ghazoui, Z., Bertrand, S., Vanneste, K., Yokoyama, Y., Beek, P., 2019. Potentially Large post-1505 AD Earthquakes in Western Nepal Revealed by a lake Sediment Record. Nat. Commun. 10, 2258. https://doi.org/10.1038/s41467-019-10093-4.

Han, W.X., Fang, X.M., Yang, S.L., King, J., 2010. Differences between east Asian and Indian monsoon climate records during MIS3 attributed to differences in their driving mechanisms: Evidence from the loess record in the Sichuan basin, southwestern China and other continental and marine climate records. Quat. Int. 218, 94-103. https://doi.org/10.1016/j.quaint.2010.01.002.

Heermance, R.V., Chen, J., Burbank, D.W., Wang, C.S., 2007. Chronology and tectonic controls of Late Tertiary deposition in the southwestern Tian Shan foreland, NW China. Basin Res. 19, 599-632. https://doi.org/10.1111/j.1365-2117.2007.00339.x.

Howarth, J.D., Fitzsimons, S.J., Norris, R.J., Langridge, R., Vandergoes, M.J., 2016. A 2000 yr rupture history for the alpine fault derived from lake Ellery, South Island, New Zealand. Geol. Soc. Am. Bull. 128, 627–643. https://doi.org/10.1130/B31300.1.

Hu, X.M., Garzanti, E., Wang, J.G., Huang, W.T., An, W., Webb, A., 2016. The timing of India-Asia collision onset-Facts, theories, controversies. Earth Sci. Rev. 160, 264-299. https://doi.org/10.1111/j.1365-2117.2007.00339.x.

Huang, B.C., Piper, J.D.A., Qiao, Q.Q., Wang, H.L., Zhang, C.X., 2010. Magnetostratigraphic and rock magnetic study of the Neogene upper Yaha section, Kuche Depression (Tarim Basin): Implications to formation of the Xiyu conglomerate formation, NW China. J. Geophys. Res. Solid Earth 115, B01101. https://doi.org/10.1029/2008JB006175.

Hubbard, J., Shaw, J.H., 2009. Uplift of the Longmen Shan and Tibetan plateau, and the 2008 Wenchuan (M=7.9) earthquake. Nature 458, 194-197. https://doi.org/10.1038/nature07837.

Jiang, H., Zhang, J., Zhang, S., Zhong, N., Wan, S., Alsop, G.I., Xu, H., Guo, Q., Yan, Z., 2022. Tectonic and climatic impacts on environmental evolution in East Asia during the Palaeogene. Geophys. Res. Lett. 49, e2021GL096832. https://doi.org/10.1029/2021GL096832.

Jiang, H.C., Ding, Z.L., 2008. A 20 Ma pollen record of East-Asian summer monsoon evolution from Guyuan, Ningxia, China. Palaeogeogr. Palaeoclimat. Palaeoecol. 265, 30-38. https://doi.org/10.1016/j.palaeo.2008.04.016.

Jiang, H.C., Guo, G.X., Cai, X.M., Xu, H.Y., Ma, X.L., Zhong, N., Li, Y.H., 2013. A pollen record of the Mid-Pleistocene Transition from Beijing, North China. J. Quat. Sci. 28, 720-728. https://doi.org/10.1002/jqs.2661.

Jiang, H.C., Mao, X., Xu, H.Y., Thompson, J., Wang, P., Ma, X.L., 2011. Last glacial pollen record from Lanzhou (Northwestern China) and possible forcing mechanisms for the MIS 3 climate change in Middle to East Asia. Quat. Sci. Rev. 30, 769-781. https://doi.org/10.1016/j.quascirev.2010.12.024.

Jiang, H.C., Mao, X., Xu, H.Y., Yang, H.L., Ma, X.L., Zhong, N., Li, Y.H., 2014. Provenance and earthquake signature of the last deglacial Xinmocun lacustrine sediments at Diexi, East Tibet. Geomorphology 204, 518-531. https://doi.org/10.1016/j.geomorph.2013.08.032.

Jiang, H.C., Shevenell, A., Yu, S., Xu, H.Y., Mao, X., 2015. Decadal- to centennial-scale East Asian summer monsoon variability during the Medieval Climate Anomaly reconstructed from an eastern Tibet lacustrine sequence. J. Paleolimnol. 54, 205–222. https://doi.org/10.1007/s10933-015-9847-1

Jiang, H.C., Zhong, N., Li, Y.H., Ma, X.L., Xu, H.Y., Shi, W., Zhang, S.Q., Nie, G.Z., 2017. A continuous 13.3-ka record of seismogenic dust events in lacustrine sediments in the eastern Tibetan Plateau. Scientific Reports 7:15686, https://doi.org/10.1038/s41598-017-16027-8.

Jiang, H.C., Zhong, N., Li, Y.H., Xu, H.Y., Yang, H.L., Peng, X.P., 2016. Soft Sediment Deformation Structures in the Lixian Lacustrine Sediments, Eastern Tibetan Plateau and Implications for Postglacial Seismic Activity. Sediment. Geol. 344, 123-134. https://doi.org/10.1016/j.sedgeo.2016.06.011.

Jing, S.W., Wang, F.D., Capezzuoli, E., Huang, G.Q., Li, J.H., Jiang, H.C., Zhou, Z.J., Zhao, X.Q., Dong, F.Q. and Brogi, A., 2023. Characteristics of seismogenic dust particles from a mountain and their significance for paleoseismic records in a tufa section: A case study of Jiuzhaigou, China. Minerals 2023, 13, 981. https://doi.org/10.3390/min13070981

Jiang, H.C., Xu, C., Adhikari, B.R., Liu, X.Q., Tan, X.B. and Yuan, R.M., 2022b. Editorial: Environmental change driven by climatic change, tectonism and landslide. Front. Earth Sci. 10:1076801. doi: 10.3389/feart.2022.1076801

Jordan, T.E., Flemings, P.B., Beer, J.A., 1988. Dating thrust-fault activity by use of foreland-basin strata. In: Paola, C. and Kleinspehn, K.L., (Eds.), New perspectives in basin analysis, New York, Springer-Verlag, p.307-330. https://doi.org/10.1007/978-1-4612-3788-4_16.

Karlin, R.E., Abella, S.E.B., 1992. Paleoearthquakes in the Puget Sound region recorded in sediments from Lake Washington, U.S.A. Science 258, 1617-1620. https://doi.org/10.1126/science.258.5088.1617.

Keefer, D. K. (1984). Landslides Caused by Earthquakes. GSA Bull. 95, 406-421. https://www.researchgate.net/publication/249525654_Landslides_caused_by_earthquakes.

Keller, E.A., Johnson, D.L., Clark, M.N., Rockwell, T. K., 1980. Tectonic geomorphology and earthquake hazard, north flank, central Ventura Basin, California. Open-File Report 81-376, U.S. Geological Survey https://doi.org/10.3133/ofr81376.

Keller, E.A., Pinter, N., 2002. Active Tectonics: Earthquakes, Uplift and Landscape. 2nd ed.; Prentice Hall: Upper Saddle River, New Jersey, USA.

Kirby, E., Reiners, P.W., Krol, M.A., Whipple, K.X., Hodges, K.V., Farley, K.A., Tang, W., Chen, Z., 2002. Late Cenozoic evolution of the eastern margin of the Tibetan Plateau: Inferences from 40Ar/39Ar and (U-Th)/He thermochronology. Tectonics 21, 1001. https://doi.org/10.1029/2000TC001246.

Kirby, E., Whipple, K., Harkins, N., 2008. Topography reveals seismic hazard. Nat. Geosci. 1, 485-487. https://doi.org/10.1038/ngeo265.

Kirby, E., Whipple, K.X., 2003. Distribution of active rock uplift along the eastern margin of the Tibetan Plateau: Inferences from bedrock channel longitudinal profiles. J. Geophys. Res. 108, 2217. https://doi.org/10.1029/2001jb000861

Kirkpatrick, H.M., Moon, S., Yin, A., Harrison, T.M., 2021. Impact of fault damage on eastern Tibet topography. Geology 49, 30-34. https://doi.org/10.1130/G48179.1.

Levi, T., Weinberger, R., Aifa, T., Eyal, Y., Marco, S., 2006. Earthquake-induced clastic dikes detected by anisotropy of magnetic susceptibility. Geology 34, 69-72. https://doi.org/10.1130/G22001.1.

Li, G., West, A.J., Densmore, A.L., Jin, Z., Parker, R.N., Hilton, R.G., 2014. Seismic mountain building: Landslides associated with the 2008 Wenchuan earthquake in the context of a generalized model for earthquake volume balance. Geochem. Geophys. Geosyst. 15, 833-844. https://doi.org/10.1002/2013GC005067.

Li, J.F., Xie, G., Yang, J., Ferguson, D.K., Liu, X.D., Liu, H., Wang, Y.F., 2020. Asian Summer Monsoon changes the pollen flow on the Tibetan Plateau. Earth Sci. Rev. 202, 103114. https://doi.org/10.1016/j.earscirev.2020.103114.

Li, Y., Craven, J., Schweig, E.S., Obermeier, S.F., 1996. Sand boils induced by the 1993 Mississippi River flood: Could they one day be misinterpreted as earthquake-induced liquefaction?. Geology 24, 171-174. https://doi.org/10.1130/0091-7613(1996)024<0171:sbibtm>2.3.co;2.

Li, Y., Zhou, R.J., Densmore, A.L., Ellis, M.A., 2006. Geomorphic evidence for the Late Cenozoic strike-slipping and thrusting in Longmen Mountain at the eastern margin of the Tibetan Plateau. Quat. Sci. 26, 40-51. https://doi.org/10.3321/j.issn:1001-7410.2006.01.006 (in Chinese with English abstract).

Liang, L.J., Jiang, H.C., 2017. Geochemical composition of the last deglacial lacustrine sediments in East Tibet and implications for provenance, weathering and earthquake events. Quat. Int. 430, 41-51. https://doi.org/10.1016/j.quaint.2015.07.037.

Liang, L.J., Qiao, X.F., Dai, F.C., Zhong, N., Jiang, H.C., 2021. Seismically triggered soft-sediment deformation structures in Tashkorgan lacustrine sediments, northeastern Pamir, China. Quat. Int. 604, 82-92. https://doi.org/10.1016/j.quaint.2021.06.021.

Liu, M., 2014. Research on the risk stone under wind loading with wind tunnel test in the Min River Valley. Chengdu University of Technology, Sichuan (master thesis), 1-95.

Liu, Q.Y., van der Hilst, R.D., Li, Y., Yao, H.J., Chen, J.H., Guo, B., Qi, S.H., Wang, J., Huang, H., Li, S.C., 2014. Eastward expansion of the Tibetan Plateau by crustal flow and strain partitioning across faults. Nat. Geosci. 7, 361-365. https://doi.org/10.1038/ngeo2130.

Liu, W.M., Carling, P.A., Hu, K.H., Wang, H., Zhou, Z., Zhou, L.Q., Liu, D.Z., Lai, Z.P., Zhang, X.B., 2019. Outburst floods in China: A review. Earth Sci. Rev. 197, 102895. https://doi.org/10.1016/j.earscirev.2019.102895.

Ma, B.Q., Su, G., Hou, Z.H., Shu, S.B., 2005. Late Quaternary slip rate in the central part of the Longmenshan fault zone from terrace deformation along the Minjiang River. Seismol. Geol. 27, 234-242 (in Chinese with English abstract).

Ma, J.X., Chen, J., Cui, Z.J., Zhou, W.D., Liu, C., Guo, P., Shi, Q., 2018. Sedimentary evidence of outburst deposits induced by the Diexi paleolandslide-dammed lake of the upper Minjiang River in China. Quat. Int. 464, 460-481. https://doi.org/10.1016/j.quaint.2017.09.022.

Marco, S., Agnon, A., 1995. Prehistoric earthquake deformations near Masada, Dead Sea graben. Geology 23, 695-698. Marco, Shmuel; Agnon, Amotz (1995). Prehistoric earthquake deformations near Masada, Dead Sea graben. Geology, 23, 695-698. https://doi.org/10.1130/0091-7613(1995)023<0695:PEDNMD>2.3.CO;2.

Mchugh, C.M.G., Seeber, L., Cormier, M.H., Dutton, J., Polonia, A., 2006. Submarine earthquake geology along the north Anatolia Fault in the Marmara Sea, Turkey: a model for transform basin sedimentation. Earth Planet. Sci. Lett. 248, 661-684. https://doi.org/10.1016/j.epsl.2006.05.038.

Moussavi-Harami, R., Mahboubi, A., Khanehbad, M., 2004. Analysis of controls on downstream fining along three gravel-bed rivers in the Band-e-Golestan drainage basin NE Iran. Geomorphology 61, 143-153. https://doi.org/10.1016/j.geomorph.2003.12.005.

Obermeier, S.F., Bleuer, N.R., Munson, C.A., Munson, P.J., Martin, W.S., McWilliams, K.M., Tabaczynski, D.A., Odum, J.K., Rubin, M., Eggert, D.L., 1991. Evidence of strong earthquake shaking in the lower Wabash valley from prehistoric liquefaction features. Science 251, 1061-1063. https://doi.org/10.1126/science.251.4997.1061.

Ou, X.J., Zhen, L.H., Zhou, S.Z., Lai, Z.P., 2012. A review on research of loess and environmental change in west Sichuan Plateau of the eastern Qinghai-Tibetan Plateau. J. Earth Environ. 3, 692-704 (in Chinese with English abstract).

Ouimet, W.B., 2007. Dissecting the eastern margin of the Tibetan Plateau: A study of landslides, erosion and river incision in a transient landscape. Ph.D. thesis, Cambridge, Massachusetts Institute of Technology, p 197.

Paola, C., Heller, P.L., Angevine, C.L., 1992a. The large-scale dynamics of grain-size variation in alluvial basins: 1. Theory. Basin Res. 4, 73-90. https://doi.org/10.1111/j.1365-2117.1992.tb00145.x.

Paola, C., Parker, G., Seal, R., Sinha, S.K., Southard, J.B., Wilcock, P.R., 1992b. Downstream fining by selective deposition in a laboratory flume. Science 258, 1757-1760. https://doi.org/10.1126/science.258.5089.1757.

Parish, T.R., 1988. Surface winds over the Antarctic continent: A review. Rev. Geophys. 26, 169-180. https://doi.org/10.1029/rg026i001p00169.

Parish, T.R., Bromwich, D.H., 1987. The surface windfield over the Antarctic ice sheets. Nature 328, 51-54. https://doi.org/10.1038/328051a0.

Parsons, T., Ji, C., Kirby, E., 2008. Stress changes from the 2008 Wenchuan earthquake and increased hazard in the Sichuan basin. Nature 454, 509-510. https://doi.org/10.1038/nature07177.

Ren, J.J., Xu, X.W., Zhang, S.M., Yeats, R.S., Chen, J.W., Zhu, A.L. Liu, S., 2018. Surface rupture of the 1933 M 7.5 Diexi earthquake in eastern Tibet: implications for seismogenic tectonics. Geophys. Jo. Inter. 212 1627–44. https://doi.org/10.1093/gji/ggx498.

Ren, Z.K., Zhang, Z.Q., Zhang, H.P., Zheng, W.J., and Zhang, P.Z., 2018b. The role of the 2008 Mw 7.9 Wenchuan earthquake in topographic evolution: seismically induced landslides and the associated isostatic response. Tectonics 37, 2748-2757

Rinat, Y., Matmon, A., Arnold, M., Aumaitre, G., Bourles, D., Deddadouche, K., Porat, N., Morin, E., Finkel, R.C., 2014. Holocene rockfalls in the southern Negev Desert, Israel and their relation to Dead Sea fault earthquake. Quat. Res. 81, 260-273. https://doi.org/10.1016/j.yqres.2013.12.008.

Romans, B.W., Castelltort, S., Covault, J.A., Fildani, A., Walsh, J.P., 2016. Environmental signal propagation in sedimentary systems across timescales. Earth Sci. Rev. 153, 7-29. https://doi.org/10.1016/j.earscirev.2015.07.012.

Schwartz, D.P., Coppersmith, K.J., 1984. Fault behavior and characteristic earthquakes: Examples from the Wasatch and San Andreas faults. J. Geophys. Res. 89, 5681-5698. https://doi.org/10.1029/JB089iB07p05681.

Seal, R., Paola, C., Parker, G., ASCE Member, Southard, J.B., Wilcock, P.R., 1997. Experiments on downstream fining of gravel: I. narrow-channel runs. J. Hydraulic Eng. 123, 874-884. https://doi.org/10.1061/(ASCE)0733-9429(2000)126:3(198).

Shen, Z.K., Sun, J.B., Zhang, P.Z., Wan, Y.G., Wang, M., Burgmann, R., Zeng, Y.H., Gan, W.J., Liao, H. Wang, Q.L., 2009. Slip maxima at fault junctions and rupturing of barriers during the 2008 Wenchuan earthquakes. Nat. Geosci. 2, 718-724. https://doi.org/10.1038/ngeo636.

Shi, W., Jiang, H.C., Alsop, G.I. Wu, G., 2022a. A continuous 13.3-ka paleoseismic record constrains major earthquake recurrence in the Longmen Shan collision zone. Front. Earth Sci. 10:838299. https://doi.org/10.3389/feart.2022.838299.

Shi, W., Jiang, H.C., Liang, L.J., Xu, H.Y., Fan, J.W., 2023. Factors controlling the spatiotemporal variability of dust magnetic susceptibility across the Chinese Loess Plateau and eastern Tibetan Plateau. Quat. Int. 661, 1-9. https://doi.org/10.1016/j.quaint.2023.04.005.

Shi, W., Jiang, H.C., Mao, X., Xu, H.Y., 2020. Pollen record of climate change during the last deglaciation from the eastern Tibetan Plateau. PLoS ONE 15, e0232803. https://doi.org/10.1371/journal.pone.0232803.

Shi, W., Jiang, H.C., Xu, H.Y., Ma, S.Y., Fan, J.W., Zhang, S.Q., Guo, Q.Q., Wei, X.T., 2022b. Response of modern fluvial sediments to regional tectonic activity along the upper Min River, eastern Tibet. Earth Surf. Dyn. 10, 1195-1209. https://doi.org/10.5194/esurf-10-1195-2022.

Si, S.P., Li, Y.L., Lu, S.H., Wang, Y.R., 2014. Holocene slip rate and paleoearthquake records of the Salt Lake segment of the Northern Zhongtiaoshan Fault, Shanxi Province. Sci. China (Earth Sci.) 57, 2079-2088. https://doi.org/10.1007/s11430-014-4887-3.

Sims, J.D., 1975. Determining earthquake recurrence intervals from deformational structures in young lacustrine sediments. Tectonophysics 29, 141-152. https://doi.org/10.1016/0040-1951(75)90139-0.

Singer, M.B., 2010. Transient response in longitudinal grain size to reduced gravel supply in a large river. Geophys. Res. Lett. 37, L18403. https://doi.org/10.1029/2010GL044381.

Sklar, L., Dietrich, W.E., 1998. River longitudinal profiles and bedrock incision models: Stream power and the influence of sediment supply. Geophys. Monogr. Ser., 107, 237-260. https://doi.org/10.1029/GM107p0237

Su, L.J., Hu, K.H., Zhang, W.F., Wang, J., Lei, Y., Zhang, C.L., Cui, P., Alessandro, P., Zhang, Q.H., 2017. Characteristics and triggering mechanism of Xinmo landslide on 24 June 2017 in Sichuan, China. J. Mt. Sci. 14, 1689-1700. https://doi.org/10.1007/s11629-017-4609-3.

Sukhija, B.S., Rao, M.N., Reddy, D.V., Nagabhushanam, P., Hussain, S., Chadha, R.K., Gupta, H.K., 1999. Paleoliquefaction evidence and periodicity of large prehistoric earthquakes in Shillong Plateau, India. Earth Planet. Sci. Lett. 167, 269-282. https://doi.org/10.1016/S0012-821X(99)00015-1.

Sun, J.B., Yue, H., Shen, Z.K., Fang, L.H., Zhan, Y., Sun, X.Y., 2018. The 2017 Jiuzhaigou earthquake: a complicated event occurred in a young fault system. Geophys. Res. Lett. 45, 2230-2240. https://doi.org/10.1002/2017GL076421.

Sun, J.M., Zhu, R.X., An, Z.S., 2005. Tectonic uplift in the northern Tibetan Plateau since 13.7 Ma ago inferred from molasses deposits along the Altyn Tagh Fault. Earth Planet. Sci. Lett. 235, 641-653. https://doi.org/10.1016/j.epsl.2005.04.034.

Sun, J.M., Zhu, R.X., Bowler, J., 2004. Timing of the Tianshan Mountains uplift constrained by magnetostratigraphic analysis of molasses deposits. Earth Planet. Sci. Lett. 219, 239-253. https://doi.org/10.1016/S0012-821X(04)00008-1.

Turner, J., Chenoli, S.N., Samah, A., Marshall, G., Phillips, T., Orr, A., 2009. Strong wind events in the Antarctic. J. Geophys. Res. 114, D18103. https://doi.org/10.1029/2008JD011642.

Wang, M., Shen, Z.K., 2020. Present-day crustal deformation of continental China derived from GPS and its tectonic implictions. J. Geophys. Res. Solid Earth 125, e2019JB018774. https://doi.org/10.1029/2019JB018774.

Wang, P., Zhang, B., Qiu, W.L., Wang, J.C., 2011. Soft-sediment deformation structures from the diexi paleo-dammed lakes in the upper reaches of the Minjiang River, east Tibet. J. Asian Earth Sci. 40, 865-872. https://doi.org/10.1016/j.jseaes.2010.04.006.

Wei, X.T., Jiang, H.C., Xu, H.Y., Fan, J.W., Shi, W., Guo, Q.Q., Zhang, S.Q., 2021. Response of sedimentary and pollen records to the 1933 Diexi earthquake on the eastern Tibetan Plateau. Ecologic. Indicat. 129, 107887. https://doi.org/10.1016/j.ecolind.2021.107887.

Wen, M.S., Chen, H.Q., Zhang, M.Z., Chu, H.L., Wang, W.P., Zhang, N., Huang, Z., 2017. Characteristics and formation mechanism analysis of the “6·24” catastrophic landslide of the June 24 of 2017, at Maoxian, Sichuan. Chin. J. Geol. Hazard Contr. 28, 7-13. https://doi.org/10.16031/j.cnki.issn.1003-8035.2017.03.01 (in Chinese with English abstract).

Wen, X.Z., Zhang, P.Z., Du, F., Long, F., 2009. The Background of Historical and Modern Seismic Activities of the Occurrence of the 2008Ms 8.0 Wenchuan, Sichuan, Earthquake 2008 Ms 8.0 Wenchuan, Sichuan, earthquake. Chin. J. Geophys. 52, 444-454.

Wilcock, P.R., 1998. Two-fraction model of initial sediment motion in gravel-bed rivers. Science 280, 410-412. https://doi.org/10.1126/science.280.5362.410.

Xie, X.S., Zhao, J.Q., Jiang, W.L., An, W.P., Li, Z.H., Zhang, D.W., Cheng, X.Y., Gao, S.Y., Wang, C.H., Sun, C.B., Yan, C.G., 2008. Study on Holocene Paleoearthquakes in Xizhang trench on the Jiaocheng fault zone, Shanxi Province. Earthquake Research in China 22, 428-439. https://doi.org/10.3969/j.issn.0253-4967.2007.04.005.

Xu, C., 2012. Detailed inventory of landslides triggered by the 2008 Wenchuan earthquake and its comparison with other earthquake events in the world. Sci. Technol. Rev. 30, 18-26 (in Chinese with English abstract).

Xu, C., Xu, X.W., Dai, F.C., Xiao, J.Z., Tan, X.B., Yuan, R.M., 2012. Landslides hazard mapping using GIS and weight of evidence model in Qingshui River watershed of 2008 Wenchuan earthquake struck region. J. Earth Sci. 23, 97-120. https://doi.org/10.1007/s12583-012-0236-7.

Xu, C., Xu, X.W., Yao, X., Dai, F.C., 2013. Three (nearly) complete inventories of landslides triggered by the May 12, 2008 Wenchuan Mw 7.9 earthquake of China and their spatial distribution statistical analysis. Landslides 11, 441-461. http://dx.doi.org/10.1007/s10346-013-0404-6.

Xu, H., Chen, J., Cui, Z.J., Chen, R.C., 2020. Sedimentary facies and depositional processes of the Diexi ancient dammed lake, upper Minjiang River, China. Sediment. Geol. 398, 105583. https://doi.org/10.1016/j.sedgeo.2019.105583.

Xu, H.Y., Jiang, H.C., Liu, K., Zhong, N., 2020. Potential pollen evidence for the 1933 M7.5 Diexi earthquake and implications for post-seismic landscape recovery. Env. Res. Lett. 15:094043. https://doi.org/10.1088/1748-9326/ab9af6.

Xu, H.Y., Jiang, H.C., Yu, S., Yang, H.L., Chen, J., 2015. OSL and pollen concentrate ^{14}C dating of dammed lake sediments at Maoxian, east Tibet, and implications for two historical earthquakes in AD 638 and 952. Quat. Int. 371, 290-299. https://doi.org/10.1016/j.quaint.2014.09.045.

Xu, Q., Li, W.., Dong, X.J., Xiao, X.X., Fan, X.M., Pei, X.J., 2017. The Xinmocun landslide on June 24,2017 in Maoxian, Sichuan: characteristics and failure mechanism. Chin. J. Rock Mech. Eng. 36, 2612-2028. https://doi.org/10.13722/j.cnki.jrme.2017.0855 (in Chinese with English abstract).

Xu, X.W., Wen, X.Z., Chen, G.H., and Yu, G.H., 2008. Discovery of the Longriba fault zone in Eastern Bayan Har Block, China and its tectonic implication. Sci. China ser. D: Earth Sci. 51, 1209-1223.

Xu, X.W., Wen, X.Z., Yu, G.H., Chen, G.H., Klinger, Y., Hubbard, J., Shaw, J., 2009. Coseismic reverse- and oblique-slip surface faulting generated by the 2008 Mw 7.9 Wenchuan earthquake, China. Geology 37, 515-518. https://doi.org/10.1130/G25462A.1.

Yao, T.D., Masson-Delmotte, V., Gao, J., Yu, W.S., Yang, X.X., Risi, C., Sturm, C., Werner, M., Zhao, H.B., He, Y., Ren, W., Tian, L.D., Shi, C.M., Hou, S.G., 2013. A review of climatic controls on δ18O in precipitation over the Tibetan Plateau; observations and simulations. Rev. Geophys. 51, 525-548. https://doi.org/10.1002/rog.20023.

Yeats, R.S., Prentice, C.S., 1996. Introduction to special section: Paleoseismology. J. Geophys. Res. 101, 5847-5853. https://doi.org/10.1029/95jb03134.

Zhang, F., Jin, Z.D., West, A.J., An, Z.S., Hilton, R.G., Wang, J., Li, G., Densmore, A.L., Yu, J.M., Qiang, X.K., Sun, Y.B., Li, L.B., Gou, L.F., Xu, Y., Xu, X.W., Liu, X.X., Pan, Y.H., You, C.F., 2019. Monsoonal control on a delayed response of sedimentation to the 2008 Wenchuan earthquake. Sci. Adv., 5, eaav7110, https://doi.org/10.1126/sciadv.aav7110

Zhang, H.P., Liu, S.F., Yang, N., Zhang, Y.Q., Zhang, G.W., 2006. Geomorphic characteristics of the Minjiang drainage basin (eastern Tibetan Plateau) and its tectonic implications: New insights from a digital elevation model study. Island Arc, 15, 239–250. https://doi.org/10.1111/j.1440-1738.2006.00524.x

Zhang, L.Y., Xu, B., Luo, Z.W., Liao, W., 2016. Conglomerates and sandstones from the Yintun Formation in Northern Liaoning Province: Implications for the Huronian glaciation and reconstruction of the Columbia supercontinent. Sci. Bull. 61, 1384-1390. https://doi.org/10.1007/s11434-016-1141-8.

Zhang, P.Z., 2013. Beware of slowly slipping faults. Nat. Geosci. 6, 323-324. https://doi.org/10.1038/ngeo1811.

Zhang, P.Z., Wen, X.Z., Shen, Z.K., Chen, J.H., 2010. Oblique, high-angle, listric-reverse faulting and associated development of strain: the Wenchuan earthquake of May 12, 2008, Sichuan, China. Annu. Rev. Earth Planet. Sci. 38, 353-382. https://doi.org/10.1146/annurev-earth-040809-152602.

Zhang, S.Q., Jiang, H.C., Fan, J.W., Xu, H.Y., Shi, W., Guo, Q.Q., Wei, X.T., 2021. Accumulation of a last deglacial gravel layer at Diexi, eastern Tibetan Plateau and its possible seismic significance. Front. Earth Sci. 9:797732. https://doi.org/10.3389/feart.2021.797732.

Zhang, X.F., Wu, Q.J., Ding, Z.F., 2018. A P-wave velocity study beneath the eastern area of Tibetan Plateau and its implication for plateau growth. Chin. Sci. Bull. 63, 1949-1961. https://doi.org/10.1360/N972018-00337.

Zhang, X.S., Sun, S.Z., Yong, S.P., Zhuo, Z.D., Wan, R.Q., 2007. Vegetation Map of China and Its Geographic Pattern-Illustration of the Vegetation Map of the People's Republic of China (1:1000 000). Geological Press, Beijing.

Zhao, M., 2006. Dynamics of Atmospheric Boundary Layer. Beijing: Higher Education Press, p.1-350 (in Chinese with English abstract).

Zhao, X.L., Deng, Q.D., Chen, S.F., 1994. Tectonic geomorphology of the Minshan uplift in western Sichuan, Southwestern China. Seismol. Geol. 16, 429-439 (in Chinese with English abstract).

Zhao, Y., Tzedakis, P.C., Li, Q., Qin, F., Cui, Q.Y., Liang, C., Birks, H.J.B., Liu, Y.L., Zhang, Z.Y., Ge, J.Y., Zhao, H., Felde, V.A., Deng, C.L., Cai, M.T., Li, H., Ren, W.H., Wei, H.C., Yang, H.C., Zhang, J.W., Yu, Z.C., Guo, Z.T., 2020. Evolution of vegetation and climate variability on the Tibetan Plateau over the past 1.74 million years. Sci. Adv. 6, eaay6193. https://doi.org/10.1126/sciadv.aay6193.

Zhong, N., Song, X.S., Xu, H.Y., Jiang, H.C., 2017. Influence of a tectonically active mountain belt on its foreland basin: Evidence from detrital zircon dating of bedrocks and sediments from the eastern Tibetan Plateau and Sichuan Basin, SW China. J. Asian Earth Sci. 146, 251-264. https://doi.org/10.1016/j.jseaes.2017.05.035.

Zhou, R.J., Pu, X.H., He, Y.L., Li, X.G., Yi, T.Y., 2000. Recent activity of Minjiang fault zone, uplift of Minshan block and their relationship with seismicity of Sichuan. Seismol. Geol. 22, 285-294. https://doi.org/10.3969/j.issn.0253-4967.2000.03.009 (in Chinese with English abstract).

Zhou, W.J., Yu, S.Y., Burr, G., Kukla, G.J., Jull, A.J.T., Xian, F., Xiao, J.Y., Colman, S.M., Yu, H.G., Liu, Z. Kong, X.H., 2010. Postglacial changes in the Asian summer monsoon system: a pollen record from the eastern margin of the Tibetan Plateau. Boreas 39, 528-539. https://doi.org/10.1111/j.1502-3885.2010.00150.x.

Figure captions

Fig. 1. Distribution of historical earthquakes and faults on the eastern TP. The Minshan uplift zone (MUZ) is surrounded by the Huya (HYF), Minjiang (MJF), and Longmenshan fault (LMSF) zones. These three faults exhibit a slip rate of ~1 mm/year (grey arrows). The MJF shows a reverse strike component of 1 mm/year (pink arrows), while the HYF shows a reverse component of 0.5 mm/year (pink arrows). The LMSF zone shows a declining reverse component from 1.1 mm/yr in the northeast to 0.23 mm/year in the southwest (pink arrows) (Zhao et al., 1994; Zhou et al., 2000; Ma et al., 2005; Li et al., 2006; Shen et al., 2009; Sun et al., 2018). Along the MJF and HYF, eight earthquakes with M_s = 6.0-8.0 have occurred since 1900.

Fig. 2. Distribution of (a) topography and (b) rainfall on the eastern TP. (b) Min River flows from approximately north (Zhangla, Songpan) to south (Dujiangyan). Except for Sandagu and Dujiangyan, which have a maximum rainfall of 1200 mm/year, the study area is dominated by a semi-arid to arid climate (adapted from Shi et al., 2022b).

Fig. 3. Climatic characteristics of precipitation, evaporation and wind in the Upper Min River. These data can be found in the Supplementary Information.

Fig. 4. Gravel accumulation under the effects of water flow along Upper Min River. (a) Development of abrupt gravel-sand transitions (GSTs) overlies lacustrine sedimentary deposits. (b, c) Gravel accumulation in the middle of the Min River riverbed.

Fig. 5. Tectonically generated gravel accumulation in the Diexi Museum lacustrine deposit in the upper Min River. (a) Field photographs of Diexi Museum lacustrine deposits. (b) Two sets of gravel layers overlie the top of lacustrine sediments. (c) Intense V-shaped bending and interlayer sliding of the lacustrine layer caused by landslides. (d) Poorly rounded single-component gravel layers sandwiched between in lacustrine sediments.

Fig. 6. Tectonically-generated gravel accumulations in the Xinmocun lacustrine deposit in the upper Min River.

Fig. 7. (a) Field photographs of Xinmocun landslide. (b, c) Gravel released by the Xinmocun landslide (~4.3 million m^3; Fan et al., 2017) has been characterized as poorly sorted, angular, and uniform, and similar in composition to local bedrock.

Fig. 8. Schematic of the Foehn effect in Longmenshan Mountains. The airflow, laden with moisture in the east, rises over the mountains and then descends as a warm and dry airflow.

Fig. 9. Loess distribution (shown in orange) in the eastern TP and Sichuan Basin (adapted from Han et al., 2010; Ou et al., 2012). Note that loess gradually becomes more extensive along the upper Min River, especially upstream from Diexi.

Fig. 10. A comparison of gradient-area relationships for the three drainages is considered representative of regional variations in concavity on the eastern TP (Kirby and Whipple, 2003).

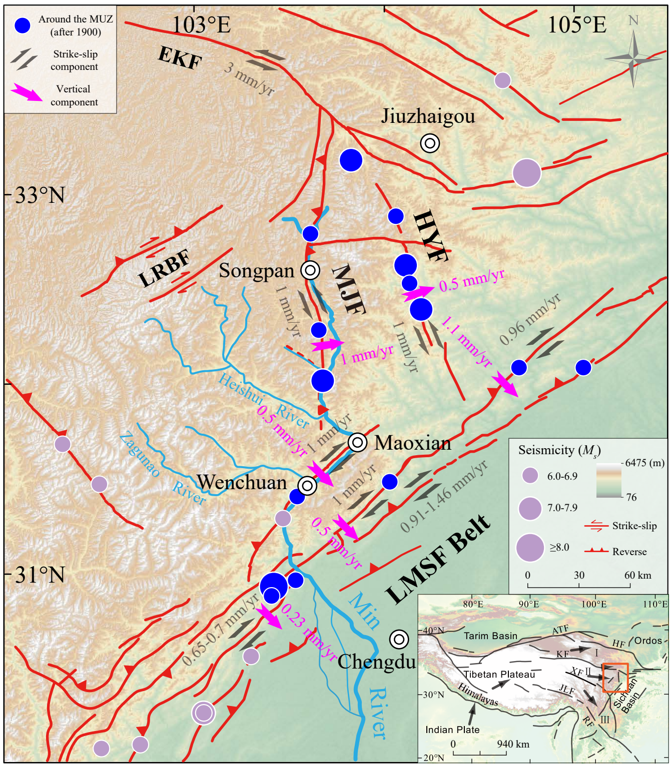

Around the MUZ (after 1900)
Strike-slip component
Vertical component
103°E
105°E
N
EKF
3 mm/yr
Jiuzhaigou
33°N
HYF
LRBF
Songpan
MJF
0.5 mm/yr
1 mm/yr
1 mm/yr
1 mm/yr
1.1 mm/yr
0.96 mm/yr
Heishui River
0.5 mm/yr
1 mm/yr
Maoxian
Zagunao River
Wenchuan
1 mm/yr
0.91-1.46 mm/yr
0.5 mm/yr
LMSF Belt
31°N
Min River
0.65-0.7 mm/yr
0.23 mm/yr
Chengdu
Seismicity (M_s)
6.0-6.9
7.0-7.9
≥8.0
6475 (m)
76
Strike-slip
Reverse
0
30
60 km
80°E
90°E
100°E
110°E
40°N
30°N
20°N
Tarim Basin
ATF
HF
Ordos
KF
Tibetan Plateau
XF
Himalayas
JLF
Sichuan Basin
RF
Indian Plate
0
940 km

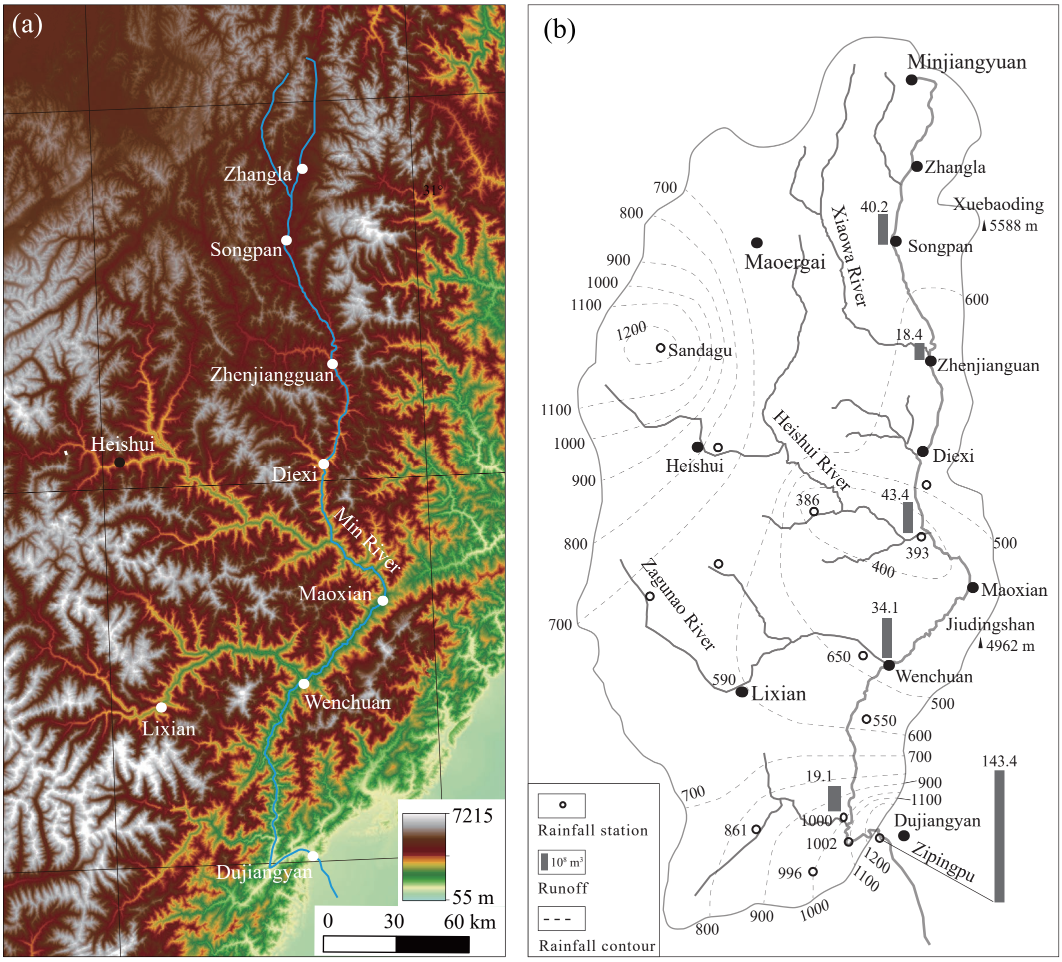

(a)
103°
104°
33°
32°
31°
Zhangla
Songpan
Zhenjiangguan
Heishui
Diexi
Min River
Maoxian
Wenchuan
Lixian
Dujiangyan
7215
55 m
0 30 60 km
(b)
Minjiangyuan
Zhangla
Xuebaoding
5588 m
Songpan
Maoergai
Xiaowa River
Sandagu
Zhenjianguan
Heishui
Heishui River
Diexi
Maoxian
Jiudingshan
4962 m
Zagunao River
Lixian
Wenchuan
Dujiangyan
Zipingpu
40.2
18.4
43.4
34.1
19.1
143.4
Rainfall station
Runoff
Rainfall contour

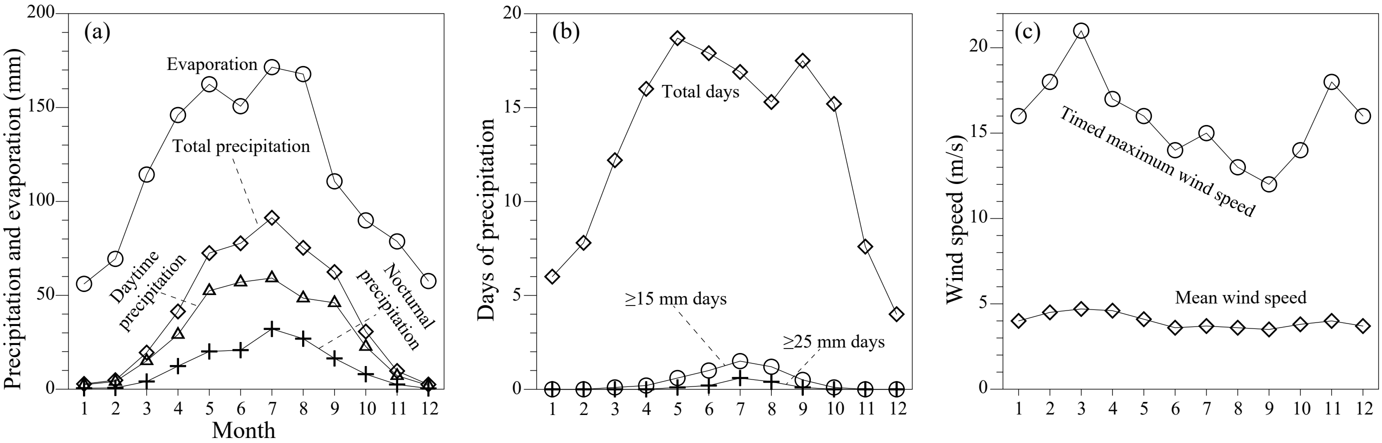

(a)
Precipitation and evaporation (mm)
Evaporation
Total precipitation
Daytime precipitation
Nocturnal precipitation
Month
(b)
Days of precipitation
Total days
≥15 mm days
≥25 mm days
(c)
Wind speed (m/s)
Timed maximum wind speed
Mean wind speed


(a)
Coarse gravel
Fine gravel
Lacustrine sediments
(b)
(c)
Min River

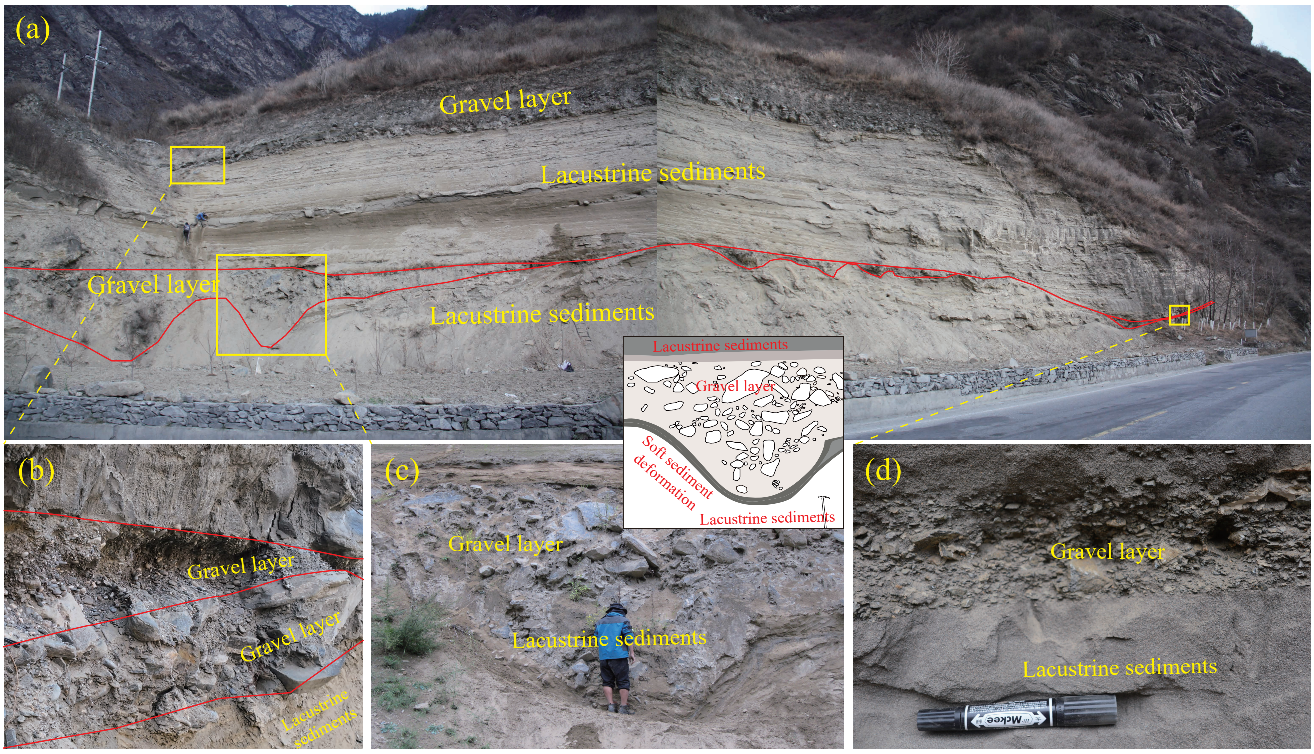
(a)
Gravel layer
Lacustrine sediments
Gravel layer
Lacustrine sediments
Lacustrine sediments
Gravel layer
Soft sediment deformation
Lacustrine sediments
(b)
Gravel layer
Gravel layer
Lacustrine sediments
(c)
Gravel layer
Lacustrine sediments
(d)
Gravel layer
Lacustrine sediments


Lacustrine sediments
Gravel layer
Lacustrine sediments
Angular gravel layer

Figure 7

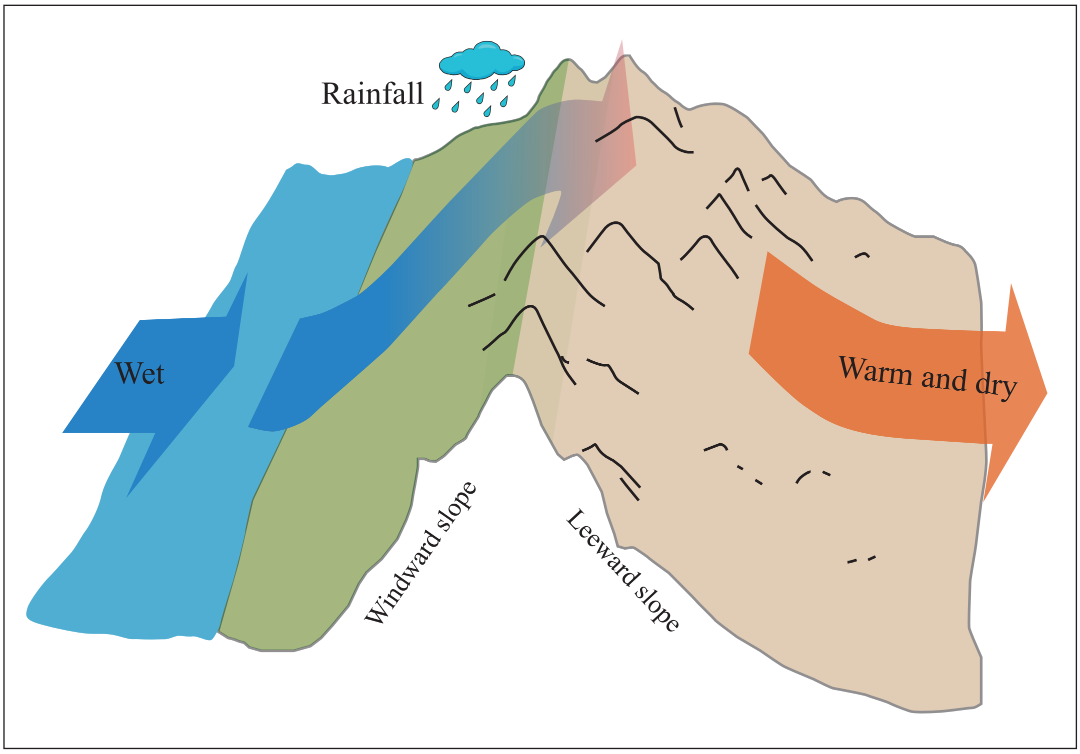

Figure 8

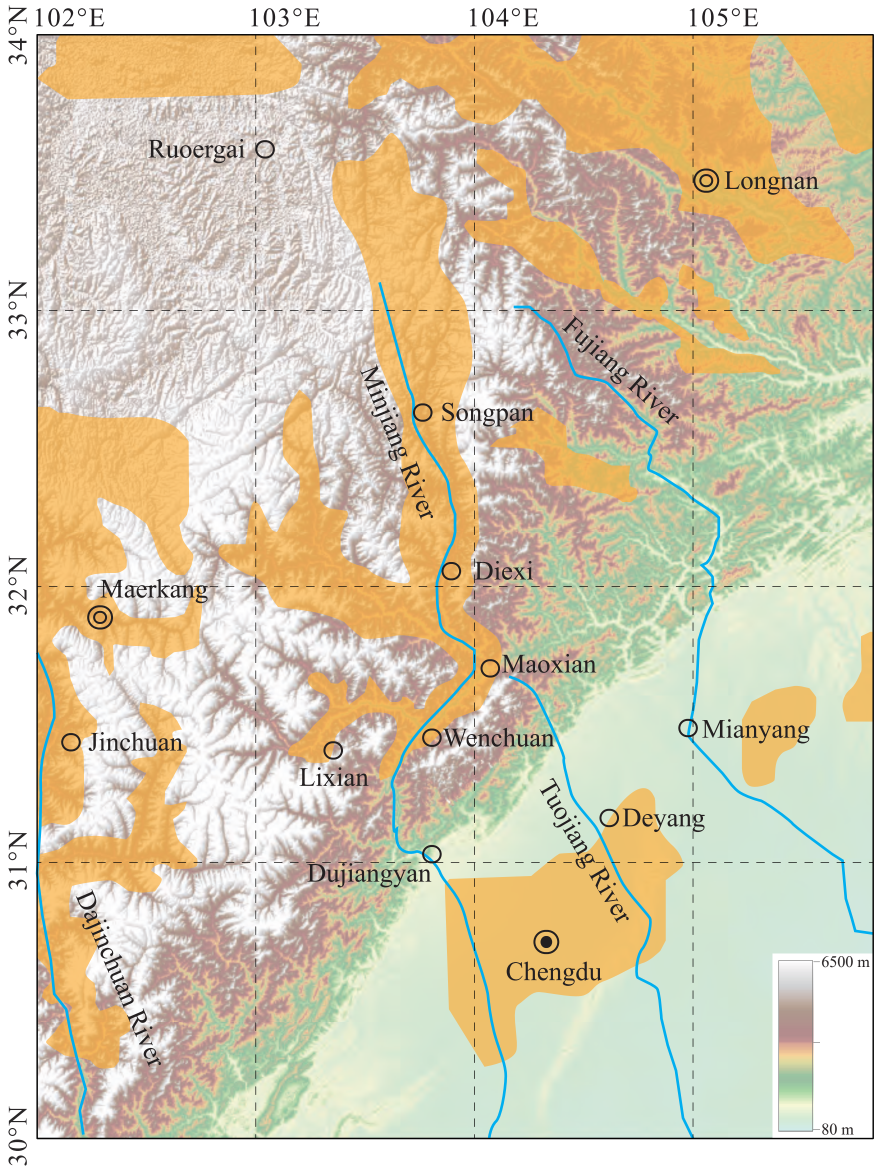
102°E
103°E
104°E
105°E
34°N
33°N
32°N
31°N
30°N
Ruoergai
Longnan
Fujiang River
Minjiang River
Songpan
Diexi
Maerkang
Maoxian
Jinchuan
Lixian
Wenchuan
Mianyang
Tuojiang River
Deyang
Dujiangyan
Dajinchuan River
Chengdu
6500 m
80 m

Figure 9

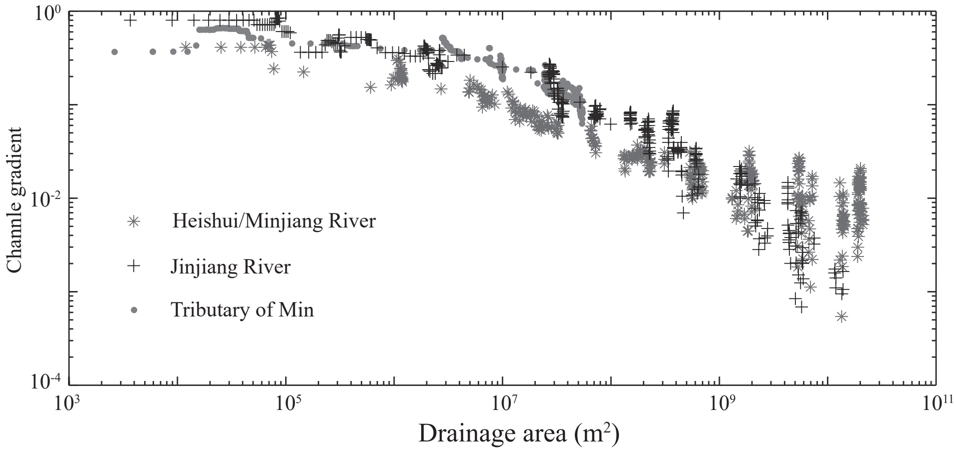

Channle gradient
Drainage area (m²)
Heishui/Minjiang River
Jinjiang River
Tributary of Min

Figure 10